European Journal of Soil Science, October 2007, **58,** 1027–1041 doi: 10.1111/j.1365-2389.2006.00882.x

Iron speciation in soils and soil aggregates by synchrotron-based X-ray microspectroscopy (XANES, μ-XANES)

J. PRIETZEL[a], J. THIEME[b], K. EUSTERHUES[a] & D. EICHERT[c]
[a]*Lehrstuhl für Bodenkunde, Technische Universität München, D-85350 Freising-Weihenstephan, Germany,* [b]*Institut für Röntgenphysik, Georg-August-Universität Göttingen, Friedrich-Hund-Platz 1, 37077 Göttingen, Germany, and* [c]*X-ray Microscopy Beamline ID 21, European Synchrotron Radiation Facility, POB 220, 38043 Grenoble Cedex, France*

Summary

Iron speciation in soils is still poorly understood. We have investigated inorganic and organic standard substances, diluted mixtures of common Fe minerals in soils (pyrite, ferrihydrite, goethite), soils in a forested watershed which constitute a toposequence with a hydrological gradient (Dystric Cambisol, Dystric Planosol, Rheic Histosol), and microsites of a dissected soil aggregate by X-ray Absorption Near Edge Spectroscopy (XANES) at the iron *K*-edge (7112 eV) to identify different Fe(II) and Fe(III) components. We calculated the pre-edge peak centroid energy of all spectra and quantified the contribution of different organic and inorganic Fe-bearing compounds by Linear Combination Fitting (LCF) conducted on the entire spectrum (E = 7085–7240 eV) and on the pre-edge peak. Fe-XANES conducted on organic and inorganic standards and on synthetic mixtures of pyrite, ferrihydrite and goethite showed that by calculating the pre-edge peak centroid energy, the Fe(II)/Fe(III) ratio of different Fe-bearing minerals (Fe sulphides, Fe oxyhydroxides) in mineral mixtures and soils can be quantified with reasonable accuracy. A more accurate quantification of the Fe(II)/Fe(III) ratio was possible with LCF conducted on the entire XANES spectrum. For the soil toposequence, an increased groundwater influence from the Cambisol to the Histosol was reflected in a larger contribution of Fe(II) compounds (Fe(II) silicate, Fe monosulphide, pyrite) and a smaller contribution of Fe(III) oxyhydroxides (ferrihydrite, goethite) to total iron both in the topsoil and the subsoil. In the organic topsoils, organically bonded Fe (33–45% of total Fe) was 100% Fe(III). For different microsites in the dissected aggregate, spatial resolution of μ-XANES revealed different proportions of Fe(II) and Fe(III) compounds. Fe *K*-edge XANES and μ-XANES allows an approximate quantification of Fe(II) and Fe(III) and different Fe compounds in soils and (sub)micron regions of soil sections, such as mottles, concretions, and rhizosphere regions, thus opening new perspectives in soil research.

Introduction

Iron contributes 5.1 mass percent to the earth's crust and is a major component of many soil-forming parent materials. Consequently, primary or secondary Fe-containing minerals, such as olivine, biotite, pyrite, ferrihydrite, goethite, haematite, lepidocrocite, and Fe-bearing clay minerals are significant components in most soils (Schwertmann & Taylor, 1989), adding up to an iron concentration between 2 and 5 g kg^{-1} in soils and more than 400 g kg^{-1} in certain soil horizons. The presence or absence of pedogenic Fe minerals in soils, soil horizons, or soil aggregates, as well as their spatial distribution within a soil profile or an aggregate is strongly related to the ambient physico-chemical conditions, such as pH, redox potential, and activity of organic ligands (e.g. Blume & Schwertmann, 1969; Cornell & Schwertmann, 1996). *Vice versa*, soil physico-chemical conditions are greatly influenced by Fe-containing minerals, because they can undergo redox, sorption, (de)protonation, or (co)precipitation reactions with organic and inorganic constituents of the soil solution and the soil solid phase (e.g. Schwertmann, 1993). Because most Fe minerals are strongly coloured and their presence or absence is clearly visible in soil profiles (Schwertmann & Lentze, 1966; Scheinost & Schwertmann, 1999), they have been widely used to identify

Correspondence: J. Prietzel. E-mail: prietzel@wzw.tum.de
Received 7 June 2006; revised version accepted 16 October 2006

pedogenic processes (podzolisation, gleysation, lessivage), and to classify soils (Blume & Schwertmann, 1969; Schwertmann, 1993).

As a consequence of the considerable importance of Fe-containing minerals in earth sciences, their identification and quantification in geologic materials and soils has been a major target of research, and numerous methods for the assessment of Fe minerals in soils have been developed. These methods include X-ray diffraction (Schwertmann *et al*., 1982), wet chemical fractionation procedures (selective extraction; Mehra & Jackson, 1960; Schwertmann, 1964; Holmgren, 1967), differential thermal analysis, Moessbauer spectroscopy (Schwertmann *et al*., 1982), or colorimetry (Schwertmann & Lentze, 1966; Scheinost & Schwertmann, 1999). However, most of these methods are either applicable only to crystalline phases (XRD) or provide only operationally defined results (dissolution methods). Moreover, none of these methods provides information on the micromorphological arrangement of different Fe species in natural soil structures, e.g. aggregates, etc.

In recent years, synchrotron-based X-ray absorption near edge spectroscopy (XANES) has been introduced as a tool for the speciation of various elements in soil extracts, particle size separates, and soils. XANES at the Fe *K*-edge (7112 eV) is sensitive to the oxidation state of Fe, but also provides information about the local chemical and structural environment. Recent studies showed that Fe *K*-edge XANES can be used to identify and quantify different Fe-containing minerals in rocks and glasses (Bajt *et al*., 1994; Delaney *et al*., 1998; Dyar *et al*., 2001, 2002; Wilke *et al*., 2001; Bonnin-Mosbah *et al*., 2002), and also can be applied to soils (cf. LaForce & Fendorf, 2000). Recently, Bonnin-Mosbah *et al*. (2002) combined spatially resolving XANES (μ-XANES) with spatially resolving X-ray fluorescence spectroscopy (μ-XRF) and X-ray microscopy for the Fe speciation of basaltic glass inclusions in olivine grains. Prietzel *et al*. (2003) used that combination for the speciation of S at different microsites of soil particles. Hence, this method should also allow a spatially resolved Fe-speciation in soil particles and soil aggregates. In summary, Fe *K*-edge XANES conducted on soils might be useful for the validation of operationally defined routine procedures of Fe speciation (LaForce & Fendorf, 2000) and may also help to elucidate the Fe speciation of soil particles and soil aggregates on a micron or submicron scale. In the following we demonstrate (i) the ability of Fe *K*-edge XANES to identify and quantify different Fe species in bulk soils, and (ii) the ability of *K*-edge μ-XANES to identify and quantify different Fe species at microsites of soil aggregates.

Materials and methods

In a first experiment, Fe *K*-edge (E = 7112 eV) XANES spectra of various solid inorganic and organic Fe-containing phases relevant to soils (Table 1) were acquired. The standard substances (analytical grade) were purchased from Merck (Darmstadt, Germany) and Sigma-Aldrich (St Louis, MO, USA). The mineral specimens were either taken from the mineral collection of our institute, or provided by Professor Schwertmann (six-line ferrihydrite, goethite, schwertmannite), Dr Haubrich (Technical University of Dresden: jarosite), and Dr Scheinost (Forschungszentrum Rossendorf: marcasite, pyrrhotite).

In a second experiment, we tested the ability of Fe-XANES to identify and quantify different diluted mixtures of Fe-minerals which are frequent in anoxic and oxic soils of temperate regions. Pyrite (FeS_2) was chosen as the Fe(II)-mineral, ferrihydrite ($Fe_5HO_8{\cdot}4\ H_2O$; six-line type), and goethite (α-FeOOH), both synthesized according to Schwertmann & Cornell (1991) as pedogenic Fe(III)-minerals. Ten different mixtures of ground samples of these minerals were prepared in Fe mass ratios of 50:50:0, 80:20:0 and 33:33:33, respectively (Table 2). To simulate the Fe concentration of real soils, all mixtures were diluted with finely ground quartz (reagent grade) to a final Fe concentration of 100 mg g^{-1}. The mixtures were thoroughly homogenized in an agate mortar prior to analysis.

In a third experiment, samples taken in March 2004 from three soils in the forested Lehstenbach catchment, Fichtelgebirge, S. Germany (50°08′14″N, 11°53′07″E) with granite bedrock, described in detail by Manderscheid *et al*. (2000) and Alewell & Novak (2001), were studied. The soils came from a SE-exposed slope (elevation: 770 m a.s.l.; slope: 9°), and form a hydrological series with increasing groundwater influence. The uppermost soil is a Dystric Cambisol (WRB, 2006) with no groundwater influence. Its topsoil (0–50 cm) is oxic throughout the year; however, weak mottling in the subsoil indicates some tendency to seasonal water-logging. The second soil, situated about 50 m downhill from the Cambisol is a Dystric Planosol (WRB, 2006) affected by seasonal shallow ground-water up to the soil surface. The lowermost soil is a Rheic Histosol (WRB, 2006), which has been intensively studied and described in detail ('Schlöppnerbrunnen 1') by Paul *et al*. (2006). This soil is located in a fen, strongly influenced by shallow ground-water and subject to anoxic conditions throughout the entire year. All soils are derived from granite debris and covered with 40–50-year-old Norway spruce (*Picea abies* [L.] Karst). The granite bedrock contains only biotite, but no other primary Fe(II) silicates such as amphibole, pyroxene, or olivine (Goeman, 1972). However, weathering and soil formation have resulted in conversion of biotite into Fe-bearing secondary silicates, e.g. illite, vermiculite, and chlorite (Eusterhues *et al*., 2003), all of which can contain some Fe(II) besides the dominant Fe(III). On each site, one sample was taken from the organic topsoil (Oh, H horizon), and another from the mineral subsoil (Bw, Bg, Cr horizon). The depth and basic parameters of the horizons are described in Table 3. To avoid artificial oxidation of Fe(II), we maintained strict anoxic conditions throughout the entire process of sampling, transport, and preparation of the samples for XANES analysis. On site, soil samples were taken with a steel

Table 1 Energy positions of the pre-edge peak centroid, the inflection point of the absorption edge, and the white line of Fe K-edge XANES spectra acquired for different Fe-bearing standard substances and Fe minerals

Compound	Fe oxidation state	Centroid pre-edge peak	Inflection point absorption edge Energy position/eV	White line
Synthetic inorganic Fe compounds				
FeS	+2	7113.1	7116.6	7132.1
$FeSO_4 \cdot 5\ H_2O$	+2	7113.1	7120.5	7126.8
$FeCl_2 \cdot 4\ H_2O$	+2	7113.2	7120.5	7124.8
$Fe_2(SO_4)_3 \cdot H_2O$	+3	7114.2	7129.0	7133.4
$FeCl_3 \cdot 6\ H_2O$	+3	7114.5	7123.8	7133.4
$FePO_4 \cdot 4\ H_2O$	+3	7114.9	7125.2	7131.3
Synthetic organic Fe compounds				
Fe(II) lactate $\cdot H_2O$	+2	7112.6	7123.0	7127.2
Fe(II) oxalate $\cdot 2\ H_2O$	+2	7112.5	7121.5	7127.1
Fe(III) citrate $\cdot H_2O$	+3	7114.6	7125.1	7135.4
Fe(III) oxalate $\cdot 2\ H_2O$	+3	7114.4	7125.6	7134.9
Fe(III) EDTA	+3	7113.9	7126.1	7134.7
Fe minerals				
Pyrite	+2	7113.6	7117.9	7120.9
Pyrrhotite	+2	7113.3	7118.8	7122.0
Marcasite	+2	7113.4	7118.5	7121.4
Biotite	+2/+3	7113.8	7121.5/7125.0/7130.0	7122.9/7126.7/7131.0
Ferrihydrite	+3	7114.9	7123.2	7133.0
Goethite	+3	7115.5	7123.5	7131.5
Lepidocrocite	+3	7114.6	7123.5	7132.7
Haematite	+3	7115.0	7123.1	7133.4
Jarosite	+3	7114.7	7129.5	7131.9
Schwertmannite	+3	7115.4	7129.5	7133.1

auger and loaded within less than 1 s into 500-ml glass vessels used for freeze-drying which had been filled previously with 10 g solid CO_2 to keep the sample frozen and maintain it anoxic throughout the transport. The vessels were closed immediately with an air-tight rubber lid and flushed with pure argon (Ar) through a hole (diameter 1.5 cm) in the lid. Then the lid opening was closed with a polythene stopper with a centred hole (diameter 0.4 cm). A polythene hose (length 0.3 m) with the same diameter was attached, air-tight, to the stopper with one end, and connected to a Wolff bottle filled with O_2-free water. During the entire transport procedure, sublimation of the dry ice in the glass vessel resulted in a permanent CO_2 flux out of the vessel through the hose, thus preventing any contact of the sample with air. Within 24 hours after sampling, all samples were freeze-dried under an Ar atmosphere and finely ground in a TiO_2 ball mill in a glove box under a N_2 atmosphere (110 kPa). In the glove box, subsamples were put into 10-ml glass bottles, and the bottles were closed air-tight with a septum lid. The samples were stored under N_2 (110 kPa). For XANES analysis, 10–20 μg of ground subsample was loaded in the glove box on a sample holder (aluminium disc, diameter 3 cm, thickness 0.2 mm; with a centred circular hole [radius 0.5 mm] to carry the sample), and sealed air-tight by gluing a 4-μm thick Ultralene® foil (SPEX, CertiPrep, Metuchen, NJ, USA) over both surfaces of the sample holder. Sample thickness and homogeneity were optimized to obtain a reasonable signal-to-noise ratio in transmission, i.e. giving around 80% absorption.

In a fourth experiment, several microsites (area 0.25 μm^2) of a dissected aggregate from an epistagnic, endogleyic Phaeozem (WRB, 2006) located in a depression near Freising, Germany, under grassland (parent material: loess colluvium) were investigated by Fe *K*-edge μ-XANES and μ-XRF. From the well-aggregated, mottled Bg horizon of that soil (40–60 cm depth; organic C: 1.7%; pH: 7.0; oxalate-extractable Fe: 6.2 mg g^{-1}; dithionite-extractable Fe: 13.5 mg g^{-1}), several 1 cm^3 aggregates, which could be separated easily manually into smaller aggregates, were sampled and stored in a field-moist state under anoxic conditions as described above. Immediately before XANES analysis, the large aggregates were separated in a glove box under N_2 into smaller aggregates with sizes between 1 and 10 mm^3. A suitable aggregate (*c.* 2 mm × 2 mm × 2 mm), where visual inspection showed the penetration of a grass fine root into the aggregate interior, was carefully cut into two pieces with a scalpel, so that the aggregate edge, the root channel, and the interior part of the aggregate were part

Table 2 Ratio of Fe(II) to total Fe (Fe_t) and mixing ratio of defined mixtures of pyrite, ferrihydrite, and goethite estimated from the pre-edge peak centroid energies (PCE) of their Fe *K*-edge XANES spectra, and calculated by Linear Combination Fitting (LCF), by means of either the pre-edge peak feature or the entire XANES spectrum of the mineral mixtures and the pure minerals. Given are arithmetic mean values ± standard error

	Fe(II)/Fe_t	Fe(II)/Fe_t	Fe(II)/Fe_t LCF	Fe(II)/Fe_t LCF	Calculated percentage LCF pre-edge peak			Calculated percentage LCF entire spectrum		
	Real	PCE	Pre-edge peak	Entire spectrum	Pyrite	Ferrihydrite	Goethite	Pyrite	Ferrihydrite	Goethite
80% Pyrite/20% Ferrihydrite	0.80	0.79	0.62	0.71	61.8 ± 0.0	0.0 ± 0.0	38.2 ± 0.0	70.5 ± 0.7	0.0 ± 0.0	29.5 ± 0.7
50% Pyrite/50% Ferrihydrite	0.50	0.65	0.45	0.46	45.3 ± 0.0	0.0 ± 0.0	54.7 ± 0.0	45.4 ± 0.7	0.0 ± 0.0	54.5 ± 0.7
29% Pyrite/71% Ferrihydrite	0.29	0.40	0.52	0.16	52.9 ± 0.0	0.0 ± 0.0	47.1 ± 0.0	16.4 ± 0.9	0.0 ± 0.0	83.6 ± 0.9
80% Pyrite/20% Goethite	0.80	0.97	0.71	0.79	71.4 ± 0.0	0.0 ± 0.0	28.6 ± 0.0	79.1 ± 0.4	0.0 ± 0.0	20.9 ± 0.4
50% Pyrite/50% Goethite	0.50	0.57	0.51	0.48	50.8 ± 0.0	0.0 ± 0.0	49.2 ± 0.0	48.1 ± 0.9	0.0 ± 0.0	51.9 ± 0.9
20% Pyrite/80% Goethite	0.20	0.00	0.33	0.07	33.1 ± 0.0	0.0 ± 0.0	66.9 ± 0.0	7.1 ± 0.9	0.0 ± 0.0	92.9 ± 0.9
80% Goethite/20% Ferrihydrite	0.00	0.00	0.24	0.00	24.3 ± 0.0	0.0 ± 0.0	75.7 ± 0.0	0.0 ± 0.0	0.0 ± 2.3	100.0 ± 2.3
50% Goethite/50% Ferrihydrite	0.00	0.00	0.33	0.00	33.2 ± 0.0	0.0 ± 0.0	66.8 ± 0.0	0.0 ± 0.0	0.0 ± 1.1	100.0 ± 1.1
20% Goethite/80% Ferrihydrite	0.00	0.00	0.23	0.00	22.8 ± 0.0	0.0 ± 0.0	77.2 ± 0.0	0.0 ± 0.0	0.0 ± 1.5	100.0 ± 1.5
33% Pyrite/33% Ferrihydrite/ 33% Goethite	0.33	0.50	0.30	0.24	29.5 ± 0.0	0.0 ± 0.0	70.5 ± 0.0	23.8 ± 0.5	0.0 ± 0.0	76.2 ± 0.5

of the newly created surface. The prepared aggregate was deposited on an Ultralene® foil glued to an aluminium disc with a circular hole (radius 1.5 mm) as sample holder, after a 10-μl-drop of 1:4 Canada balsam/xylene mixture had been added as fixing agent. Within a few minutes the xylene evaporated, resulting in gradual hardening of the Canada balsam and fixation of the aggregate to the Ultralene® foil. After insertion of a spacer (thickness: 2 mm), another Ultralene® foil was glued to the top section, so that the fixed aggregate was sealed airtight by Ultralene® foils on both sides. The entire procedure was carried out in a glove box under N_2.

All experiments were conducted with the scanning transmission X-ray microscope (STXM) at beamline ID-21 of the European Synchrotron Radiation Facility (ESRF, Grenoble, France) described by Barrett *et al*. (2000) and Bonnin-Mosbah *et al*. (2002). The STXM uses a Fresnel zone plate as focusing optics, which de-magnifies the synchrotron X-ray source, produced by an electron beam (energy: 6 GeV; average current: 180 mA) to generate a submicron probe with large flux. At the Fe *K*-edge, a tungsten zone plate (Zone Plate Ltd, London, UK) was used, which provides a spatial resolution < 1 μm and a flux of 0.4×10^9 photons s^{-1} in the focused mode. The monochromaticity of the beam and the energy scan were ensured by a fixed exit double crystal Si $< 220 >$ monochromator located upstream from the microscope, which offers an energy resolution of 0.3 eV necessary to resolve the XANES structures and especially the pre-peak region of the spectrum. The X-ray transmission and fluorescence signals were recorded simultaneously with a Si photodiode mounted downstream from the sample and an energy-dispersive 30 mm^2 high-purity Ge detector (Princeton Gamma-Tech, Princeton, NJ, USA), respectively.

We obtained XANES spectra by irradiating the samples with X-rays in the energy range between 7085 and 7240 eV with stepwise increased energies in 0.25-eV increments and a dwell time (duration of irradiation with X-rays of a distinct energy) of 1 s. The intensity of transmission and fluorescence at the various energies was recorded. The spectra were usually acquired in transmission mode; in some rare cases, when the transmission signal was too weak to yield a clear spectrum, the fluorescence signal was used instead. Repeated comparisons between the transmission and the fluorescence spectra of selected samples ensured that self-absorption never constituted a problem during the XANES measurements. For each spectrum, the signals of 10 scans were summed. The energy calibration was done with pure elemental Fe foil (*K* edge: 7112 eV). We assessed the speciation of Fe in the standard substances, in the mineral mixtures, and in the bulk soil samples of the Fichtelgebirge soils by recording XANES spectra in a non-focused mode (with the zone plate removed), the size of the beam being determined by a 50-μm diameter pinhole. In this mode, a comparably large area (0.13 mm^2) of the sample was analysed, thus integrating the signal from all material in that area. Several spectra taken at different locations of the samples (distance 250 μm) were identical.

Table 3 Important properties of the horizons investigated in three soils in the Lehstenbach catchment (Fichtelgebirge, S. Germany)

Soil horizon	Depth /cm	Groundwater influence	Colour (Munsell, wet soil)	pH ($CaCl_2$)[d]	Organic C /g kg^{-1}	Fe_t[a] /g kg^{-1}	Fe_o[b] /g kg^{-1}	Fe_d[c] /g kg^{-1}
Dystric Cambisol								
Oh	3–8	None	5YR 2/2	3.4	341	9.5	ND[e]	ND
Bw	13–35	Low (< 3 months $year^{-1}$)	7.5YR 4/4	3.8	28	26.7	6.8	14.6
Dystric Planosol								
H2	5–30	Moderate (3–6 months $year^{-1}$)	5YR 2/2	3.2	298	4.7	ND	ND
Bg	58–70	Considerable (6–9 months $year^{-1}$)	10YR 6/3	4.1	16	11.9	1.1	1.1
Rheic Histosol								
H2	25–55	Permanent	5YR 2/2	3.6	375	3.5	ND	ND
Cr	72–100	Permanent	10YR 3/2	3.9	14	9.7	0.3	0.3

[a]Fe_t: total Fe, analysed by digestion with $HF/HClO_4$ and subsequent Fe analysis with ICP-OES.
[b]Fe_o: Fe extractable with acidic NH_4 oxalate (pH 3.2) according to Schwertmann (1964).
[c]Fe_d: Fe extractable with Dithionite-citrate-bicarbonate solution according to Holmgren (1967).
[d]Soil: solution ratio 1 g:10 g for Oh and H horizons, 1 g:2.5 g for B and C horizons.
[e]ND: not determined.

The XANES spectra for selected microsites on the dissected aggregate sampled from the Phaeozem were recorded in focused mode (zone plate diameter: 227 μm; outermost zone width: 100 nm; central stop diameter: 70 μm; order sorting aperture: 50 μm). In this mode, an area of 0.25 μm^2 was illuminated by the X-ray beam. In all cases, the incident beam intensity was monitored with a photodiode with a central hole inserted in the beam and measurement of the fluorescence signal from a thin 1.5 μm Al foil covering it. This so-called I_0 measurement is essential for normalizing the transmitted beam signal.

For all spectra, the energy of the white line peak (W), the absorption edge energy position (E), determined from the first maximum of the spectrum derivative (inflection point of the absorption edge), and the energy of the pre-edge peak centroid (PCE) was assessed after baseline correction and normalization for the edge step (Figure 1a). Additionally, Linear Combination Fitting (LCF) on all normalized spectra and their pre-edge peak was performed with the spectra of ferrihydrite, goethite, biotite, Fe monosulphide, pyrite, Fe(II) oxalate, and Fe(III) oxalate as predictor components for organic topsoil samples. Iron(II) and Fe(III) oxalate were selected as model compounds for organically bound soil Fe in the organic topsoils, because it is commonly accepted that organically bound Fe in soils is mainly bound to carboxylate groups of deprotonized fulvic or low-molecular weight acids such as formate, acetate, malate, citrate, and – most important – oxalate (Pohlman & McColl, 1988; Lundström *et al*., 2000). For the mineral subsoil samples, Fe(II) and Fe(III) oxalate were excluded from the LCF, because the subsoil horizons were poor in organic C, which suggests that Fe in these horizons is exclusively inorganic. Biotite was selected as model compound for six-fold coordinated Fe(II) silicates due to the great similarity of the XANES spectra of all members of that mineral class (Dyar *et al*., 2002). The LCF analyses were conducted with the software SIXpack (http://www-ssrl.slac.stanford.edu/~swebb/sixpack.htm).

Results

Standard substances

The 11 standard substances and 10 soil minerals showed clear differences in the energy positions (i) of the centroids of their normalized pre-edge peaks, (ii) of the edge energy position, and (iii) of their white lines (Table 1). Typical for XANES spectra, the less oxidized Fe(II) compounds had lower edge and white-line energy positions than the Fe(III) compounds, and also the forms of the spectra differed among the various standards and minerals (Figure 2; upper section). Thus the spectra of Fe(II) sulphides (e.g. Fe monosulphide, pyrite, marcasite) can be clearly distinguished from those of Fe(II) organic compounds, from that of biotite, and from the spectra of the Fe(III) oxyhydroxides. Moreover, FeS can be distinguished from FeS_2 minerals (pyrite, marcasite). On the other hand, the spectra of Fe(III) oxyhydroxides (haematite, goethite, ferrihydrite, and lepidocrocite) and Fe(III) organic compounds (Fe(III) oxalate, Fe(III) citrate) were very similar. The differences and similarities observed among the spectra of different Fe compounds suggest that LCF might be suitable for distinguishing among the compound classes Fe(II) sulphides, Fe(II) silicates, represented by biotite in our study, and Fe(III) oxyhydroxides in mineral mixtures and soils, whereas a discrimination among different Fe(III) oxyhydroxides appears to be difficult, if not impossible.

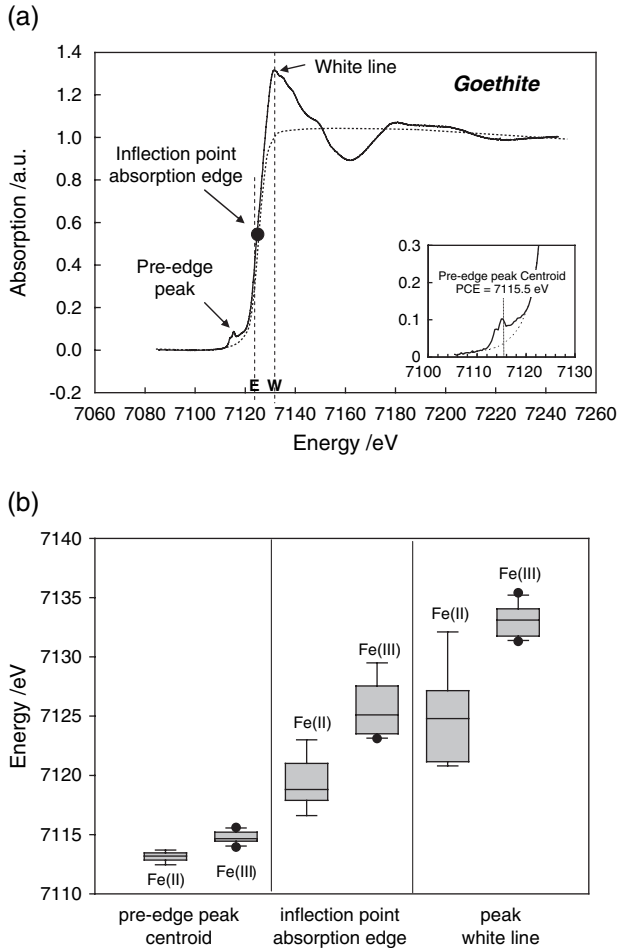

Figure 1 (a) Typical Fe *K*-edge XANES spectrum of an Fe compound (goethite; shown are the pre-edge peak, the absorption edge, and the white line). (b) Box plots of important features of Fe *K*-edge XANES spectra recorded for 8 Fe(II) and 12 Fe(III) standard and mineral compounds. The boxes represent the 25% and 75% percentiles and the median (horizontal line), the whiskers the 10 and 90% percentiles. E: energy position of the inflection point of the absorption edge. W: energy position of the white line. a.u.: arbitrary units.

The pre-edge feature (Figure 1a) can be attributed to 1s → 3d transitions of the Fe core electrons induced by illumination with X-rays of adequate energy. Even though 1s → 3d transition is an electric dipole forbidden by parity considerations, it is allowed (i) through 1s → 3d electric quadrupole coupling, and in non-centrosymmetric environments also (ii) through some 1s → 4p character in the transition caused by 3d-4p mixing with, e.g., ligands (Westre *et al*., 1997). The energy range, intensity, and shape of the pre-edge are governed by the oxidation state and the specific bonding environment of the irradiated Fe atoms (coordination type, bonding symmetry, length to neighbouring atoms; Westre *et al*., 1997; Wilke *et al*., 2001). In our study, the pre-edge peak centroid energy (PCE) positions for standards and minerals of a given Fe oxidation state class varied by < 1.5 eV, whereas the energies of the absorption edges and white lines varied within a range of at least 3 eV and up to 12 eV (Table 1; Figure 1b). A large part of the observed 1.5 eV variation of the PCE within each Fe oxidation state class is due to the fact that organic standard compounds of a given Fe oxidation state have a smaller PCE (Fe(II): 7112.5 eV; Fe(III): 7114.5 eV) than inorganic compounds (Fe(II): 7113.4 eV; Fe(III): 7114.9 eV). Thus, the PCE of mineral mixtures and soils allows an approximate quantification of their Fe(II)/Fe(III) ratio. Because also the forms of the pre-edge peak features of various standard compounds and minerals were different (Figure 2; lower section), the relative contribution of specific Fe compounds or compound classes to mineral mixtures and soils can also be assessed by Linear Combination Fitting performed on the pre-edge peak feature in addition to an LCF conducted on the entire XANES spectrum.

Mineral mixtures

The PCE of Fe *K*-edge XANES spectra of different pyrite:ferrihydrite mixtures differed by about 1.2 ± 0.4 eV (Figure 3a), and that of different pyrite:goethite mixtures (Figure 3b) by 2.0 ± 0.4 eV. This is similar to results of earlier studies of Galoisy *et al*. (2001) and Wilke *et al*. (2001), who studied the PCE of various mixtures of Fe(II) and Fe(III) silicates. Thus, an estimation of the Fe(II)/Fe(III) ratio in samples of unknown composition is possible by calculating the PCE of their normalized pre-edge peaks and comparing it with the PCE of Fe(II) and Fe(III) standards not only for mixtures, in which the coordination partner of the Fe remains the same (oxygen in the studies of Galoisy *et al*. (2001) and Wilke *et al*. (2001)), but also when it changes (from sulphur to oxygen in this study). The increase in PCE which could be observed when goethite or ferrihydrite is mixed with pyrite is due to an increased proportion of Fe(III) in the mixtures. The PCE showed a linear relationship with the ferrihydrite proportion in the pyrite:ferrihydrite mixtures (Figure 3a), whereas the relationship was not linear for pyrite:goethite mixtures (Figure 3b). The results indicate that the Fe(II)/Fe(III) ratio of pyrite:ferrihydrite or pyrite:goethite mixtures can at least be approximately quantified with the energy resolution of the instrument (0.3 eV) by calculating the PCE. In contrast, the pre-edge peak centroids of different binary mixtures of ferrihydrite and goethite showed almost identical energy positions (Figure 3c). Within a wide range of mixing ratios (20–80% goethite), the PCE varied by < 0.2 eV, which is in the range of the energy resolution of the monochromator.

For all pyrite:ferrihyrite and pyrite:goethite mixtures, the Fe(II)/Fe(III) ratio was calculated, assuming a linear increase of the PCE with an increasing proportion of Fe(III), and using the PCE of pure pyrite, goethite, and ferrihydrite as values for a contribution of 0 or 100% Fe(III), respectively. As expected from the results presented in Figure 3(a,b), the agreement between the calculated and the real Fe(II)/Fe(III) proportions

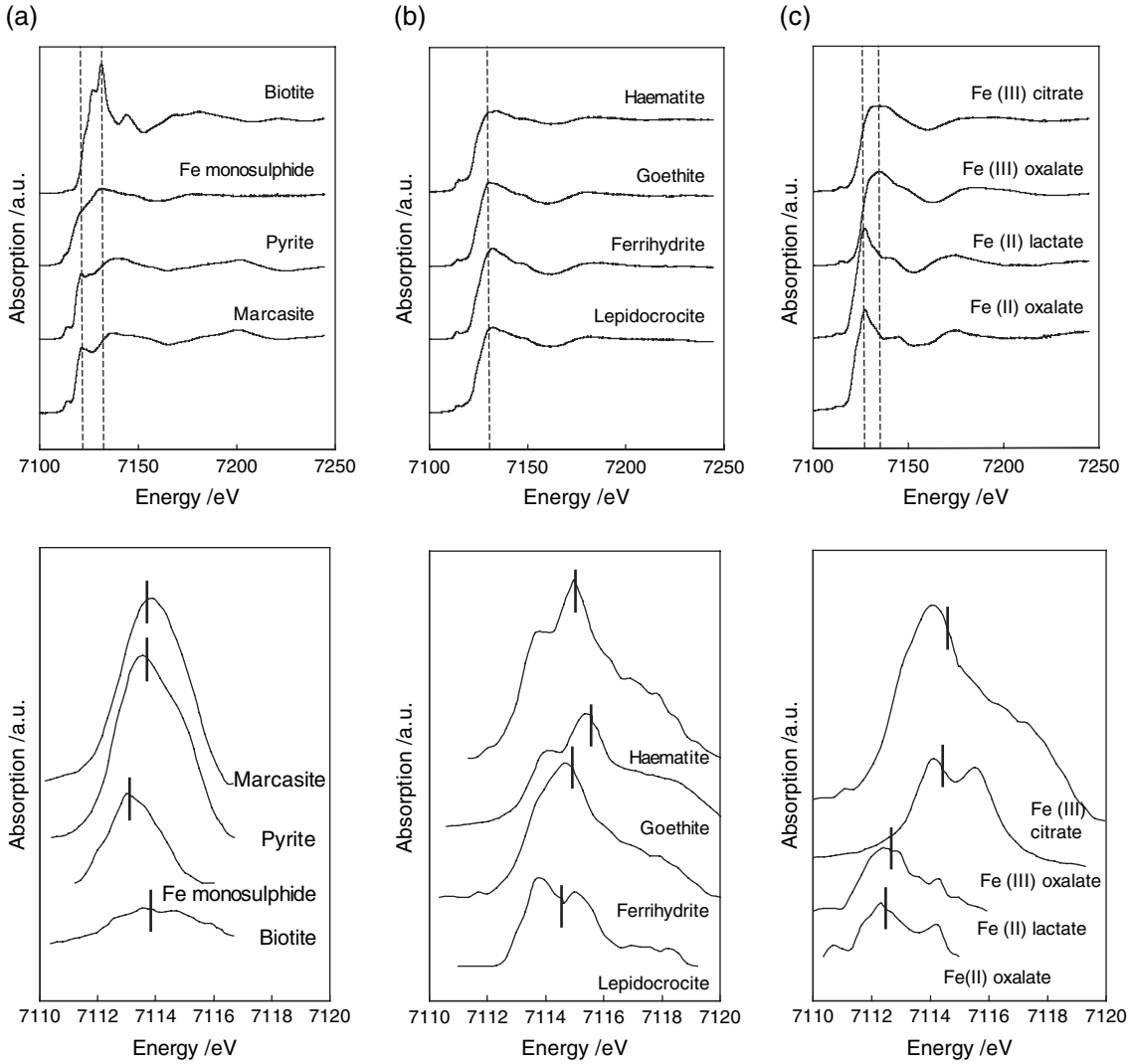

Figure 2 Fe *K*-edge XANES spectra (upper section) and their pre-edge peak features (lower section) of (a) Fe(II) minerals, (b) Fe(III) minerals, and (c) Fe(II) and Fe(III) organic complexes. Dashed lines represent the white line positions. Pre-edge peak centroid energy positions are indicated with solid bars.

(Table 2) was fairly good for the pyrite:ferrihydrite mixtures (difference between calculated and experimental Fe(II)/total Fe ratio: 1–15% of total Fe), but poor for the pyrite:goethite mixtures (difference 17–37%). In most cases, the contribution of Fe(II) was overestimated with the PCE method. When a Linear Combination Fitting (LCF) procedure was applied to the pre-edge peak features of the mineral mixtures, by means of the pre-edge peak spectra of pyrite, ferrihydrite, and goethite as independent variables, the difference between the calculated and the real contribution of Fe(II) to total Fe with 1–33% of total Fe was smaller than for the PCE approach. However, for the ferrihydrite:goethite mixtures, between 23 and 33% of total Fe were assigned erroneously to pyrite.

LCF conducted on the entire spectrum yielded the most accurate results. The calculated contribution of Fe(II) to total Fe in the various mineral mixtures generally agreed very well with the experimental contribution; in most cases it was slightly (1–13%) underestimated (Table 2). However, as for the LCF conducted on the pre-edge peak feature, ferrihydrite was always erroneously assigned to goethite. Based on these results, in the following analyses (i) LCF conducted on the entire XANES spectrum was used to calculate the contribution of Fe(II) and of different Fe-bearing compounds to total Fe in the soil samples investigated, and (ii) in these calculations no discrimination was made between goethite and ferrihydrite.

Soils with different groundwater influence

The XANES spectra of the organic topsoil horizons of the three Fichtelgebirge soils were all very similar to the spectrum of

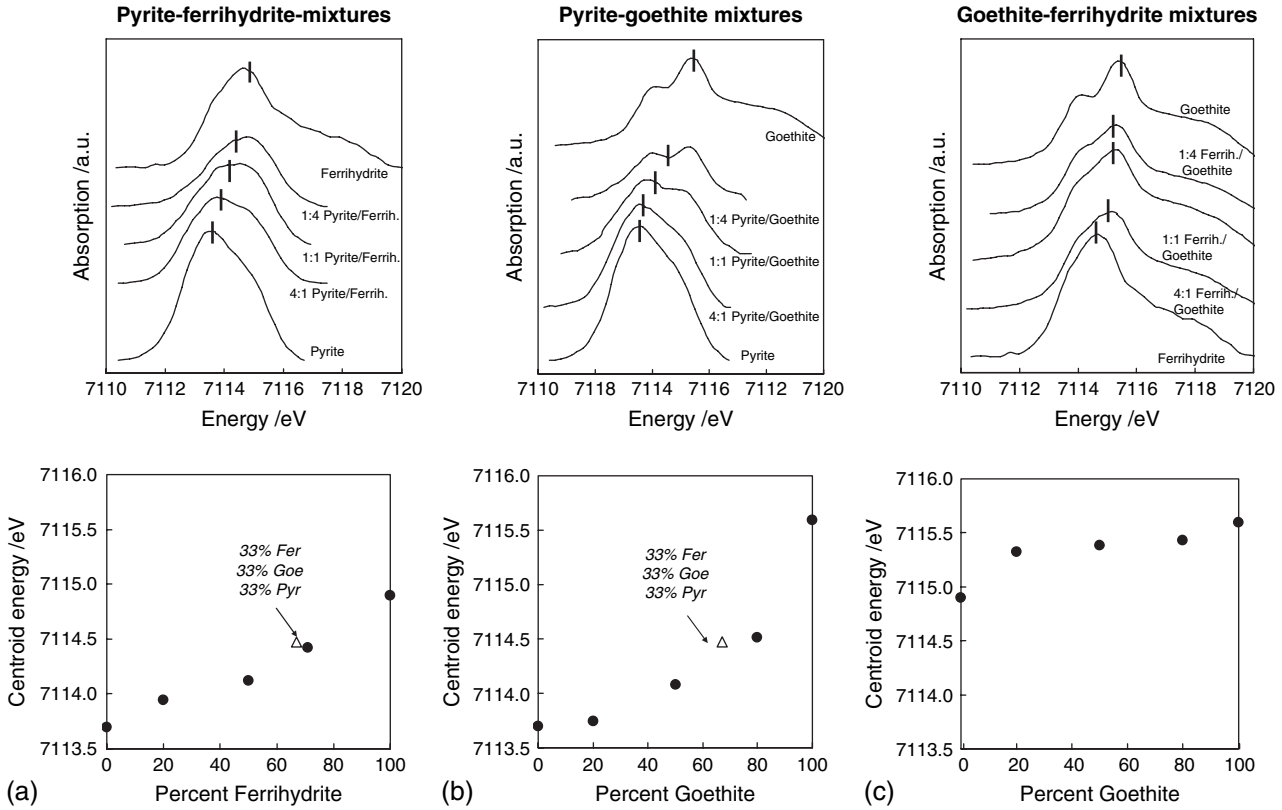

Figure 3 Fe *K*-edge XANES pre-edge peak spectra for different mixtures of (a) pyrite and 6-line ferrihydrite, (b) pyrite and goethite, and (c) goethite and 6-line ferrihydrite. Pre-edge peak centroid energy positions are indicated with solid bars.

Fe(III) oxalate (Figure 4a; upper section). However, their edges were less steep than the edge of the Fe(III) oxalate spectrum, and their pre-edge features were also different from that of pure Fe(III) oxalate (Figure 4a; lower section). With increasing groundwater influence from the Cambisol Oh to the Histosol H2 horizon, the main peak became more pronounced. Concomitantly, the pre-edge peak became less pronounced and changed its shape. The PCE shifted to a smaller energy, which indicates an increased contribution of Fe(II) from the Cambisol Oh (no Fe(II) present) to the Histosol H2 horizon (Fe(II): 36% of total Fe; Table 4). The XANES spectrum and particularly the pre-edge peak feature of the Histosol H2 horizon suggest an increased contribution of Fe(II) silicate, represented by biotite in our study, rather than of Fe(II) oxalate, Fe monosulphide, or pyrite (Figure 4). Deconvolution of the XANES spectra of the organic topsoil horizons by LCF (Table 4) showed that Fe(III) oxalate (33–53% of total Fe) and Fe(III) oxyhydroxides (24–54% of total Fe) were the dominating Fe compounds in these horizons. According to LCF, only a little Fe (1–5% of total Fe) was present as monosulphide, and no Fe existed as pyrite or Fe(II) oxalate. Thus, organically complexed Fe in all soils consisted entirely of Fe(III). From the Cambisol Oh to the Histosol H2 horizon, the contribution of Fe(II) compounds, which were mainly present as six-fold coordinated Fe silicates, increased from 13 to 23% of total Fe; the contribution of Fe oxyhydroxides decreased from 54 to 32%. Generally, the LCF results obtained for the different topsoils matched well the respective appearances of the spectra and pre-edge peak features.

The XANES spectra of the mineral soil horizons (Figure 4b) indicate a shift from a dominance of goethite or ferrihydrite in the Cambisol Bw and Planosol Bg horizons to a dominance of Fe monosulphide and pyrite in the Histosol Cr horizon. The pre-edge peak feature of the Cambisol Bw horizon had no shoulder on the high-energy side and thus resembled more the pre-edge peak of ferrihyrite than that of goethite; nevertheless, it appears to be composed by features of both Fe oxyhydroxides. The XANES spectrum and also the pre-edge peak of the Histosol Cr horizon suggest that Fe monosulphide rather than pyrite is the dominant Fe sulphide compound in that horizon. As with the organic topsoils, the white line energies and the PCEs decreased also in the mineral subsoil from the Cambisol to the Histosol, which indicates an increased contribution of Fe(II) compounds to total Fe from 19% in the Cambisol Bw horizon to 69% in the Histosol Cr horizon (Table 4). Deconvolution of the XANES spectra by LCF showed that in all soils the Fe(III) oxyhydroxides goethite or ferrihydrite were the dominant Fe compounds. However, the percentage of these minerals decreased from 100% to 59% of total Fe in the sequence Cambisol – Planosol – Histosol. Concomitantly, the percentage of Fe monosulphide increased from 0 to 26%; in the Histosol, pyrite

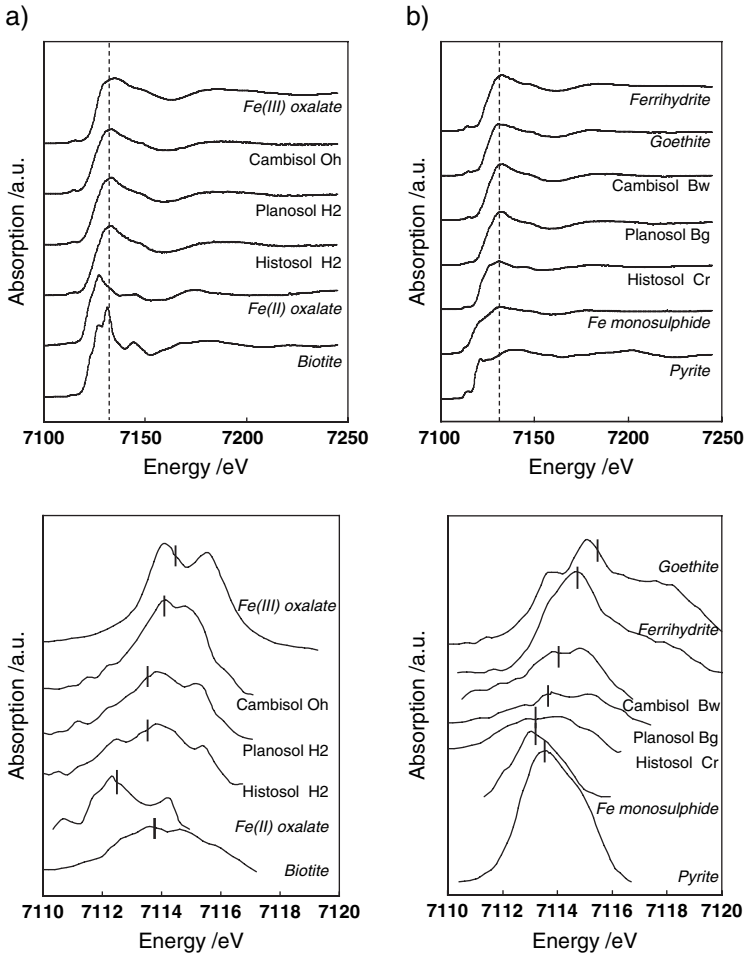

Figure 4 Fe *K*-edge XANES spectra (upper section) and their pre-edge peak features (lower section) for (a) organic topsoil horizons and (b) mineral subsoil horizons of three soils in the Fichtelgebirge, with the groundwater influence increasing in the order Dystric Cambisol – Dystric Planosol – Rheic Histosol. Pre-edge peak centroid energy positions are indicated with solid bars.

comprised an additional 15% of total Fe. The LCF results ruled out the presence of significant amounts of Fe(II) silicate minerals, represented by biotite, in the mineral soils investigated. As previously indicated by the shift of the PCE to smaller energies, also the LCF results showed an increased contribution of Fe(II) compounds to total Fe with increasing groundwater influence, i.e. from the Cambisol (no Fe(II) present) to the Histosol (Fe(II) comprising 41% of total Fe).

Aggregate

In the photographs taken of a dissected soil aggregate with an optical microscope (Figure 5a,b), the root channel (arrow in Figure 5a) could be clearly recognized. Moreover, in the interior parts of the dissected aggregate rusty-brownish mottles were visible (Figure 5a; position 1 in Figure 5b). According to the Fe fluorescence map (Figure 5c; root channel: horizontally orientated dark region in the upper section of the photograph), the rusty mottle at position 1 and also the dark regions at positions 2 and 3 were considerably enriched in Fe relative to the body of the aggregate. A manganese fluorescence map taken from the same region (not shown) revealed that the blackish region in the lower right section of Figure 5(b) was enriched in Mn, probably as Mn oxide. A comparison of the Fe XANES pre-edge peak features (Figure 5d) acquired with a focussed beam (illuminated area on the sample $< 1\ \mu m^2$) (i) at three positions with iron enrichment (positions 1, 2, 3, particularly bright in Figure 5c), (ii) in a region in the vicinity of the root channel (position 4), and (iii) in a region in the aggregate showing an average iron content (position 5), revealed differences in Fe speciation among the different microsites. The pre-edge peak feature of the XANES spectrum taken at position 1, to a lesser extent also that of position 5, were similar to those of ferrihydrite and goethite (Figure 5d). The pre-edge peaks of positions 2, 3, and 4 seemed to be combined of features of ferrihydrite, goethite, and biotite. According to their PCEs, the Fe-rich positions 1 and 2 are particularly enriched in Fe(III) relative to the other positions. The contribution of Fe(III) at positions 1 and 2 was 62 and 56% of total Fe, respectively (other positions: Fe(III) $<$ 45% of total Fe). The region close to the root channel (position 4) showed the largest percentage of Fe(II) of all investigated microsites, comprising 69% of total Fe. In most cases, the results of the PCE were confirmed by Linear Combination Fitting. As with the PCE approach, the LCF approach showed that the Fe-rich position 1 had the largest contribution

Table 4 Pre-edge peak centroid energy positions (PCE) of Fe *K*-edge XANES spectra, ratio of Fe(II)/total Fe (Fe_t), and contribution of different Fe species to Fe_t in the horizons investigated of the Fichtelgebirge soils, and at different microsites of a dissected aggregate taken from the Bg horizon of an epistagnic, endogleyic Phaeozem, as estimated from their PCE and calculated by Linear Combination Fitting (LCF) conducted on the entire Fe *K*-edge spectrum. NC: not considered: respective species considered not present in the sample and thus not included in the LCF

Sample	Energy position pre-edge peak /eV	Fe(II)/Fe_t PCE	Fe(II)/Fe_t LCF	Fe(II) oxalate	Fe(III) oxalate	Biotite	Fe monosulphide	Pyrite	Σ (Ferrihydrite + Goethite)
				/%					
Fichtelgebirge soils – organic topsoil									
Cambisol – Oh	7114.4	0.00	0.13	0	33	10	3	0	54
Planosol – H2	7114.2	0.18	0.23	0	53	18	5	0	24
Histosol – H2	7114.0	0.36	0.23	0	45	22	1	0	32
Fichtelgebirge soils – mineral subsoil									
Cambisol – Bw	7114.6	0.19	0.00	NC	NC	0	0	0	100
Planosol – Bg	7114.6	0.19	0.14	NC	NC	0	14	0	86
Histosol – Cr	7113.8	0.69	0.41	NC	NC	0	26	15	59
Soil aggregate									
Position 1 (Fe enriched)	7114.3	0.38	0.30	NC	NC	21	0	9	70
Position 2 (Fe enriched)	7114.2	0.44	0.42	NC	NC	29	0	13	58
Position 3 (Fe enriched)	7114.0	0.56	0.50	NC	NC	33	0	17	50
Position 4 (root channel)	7113.8	0.69	0.39	NC	NC	28	0	11	61
Position 5 ('average aggregate')	7114.0	0.56	0.36	NC	NC	27	0	9	64

of Fe(III) to total Fe of all sites investigated, with ferrihydrite and goethite comprising 70% of total Fe. In contrast, the Fe-rich position 3 contained 50% Fe(II) (33% biotite; 17% pyrite). Different results were obtained with both methods for position 4. Here, the PCE suggested a particularly large contribution of Fe(II) to total Fe, whereas according to the LCF analysis the Fe speciation at that microsite was similar to positions 2 and 5, the latter representing the average aggregate with regard to its Fe content.

Discussion

Assessment of the Fe(II)/Fe(III) ratio in mineral mixtures and soils based on the PCE

The Fe-XANES measurements on organic and inorganic standards show that the pre-edge peak features of their Fe *K*-edge XANES spectra, which precede the absorption edge in an energy range between 7109 and 7117 eV, and which are caused by 1s → 3d and 1s → 4p transitions of Fe core electrons (Waychunas *et al*., 1983; Westre *et al*., 1997), have a unique shape (Figure 2) and a specific PCE (Table 2) for the different standards. The differences in energy position and shape of the pre-edge peak spectra are caused by differences of (i) the oxidation state (Fe^{2+} versus Fe^{3+}), (ii) the coordination geometry (4- to 6-coordinated Fe), and (iii) the degree of Fe-octahedral polymerisation (ferrihydrite < goethite < haematite) of the irradiated Fe atoms (Waychunas *et al*., 1983; Bajt *et al*., 1994; Westre *et al*., 1997; Petit *et al*., 2001; Wilke *et al*., 2001; Guillon *et al*., 2003). Therefore, deconvolution of the pre-edge peak of a mixture of different Fe-containing compounds (e.g. a mixture of Fe minerals or a soil sample) provides information about the Fe(II)/Fe(III) ratio and the contribution of different Fe phases to the total iron content in a sample (Bajt *et al*., 1994; Petit *et al*., 2001; Wilke *et al*., 2001; Bonnin-Mosbah *et al*., 2002). In this study, we were able to quantify Fe(II) and Fe(III) in different mixtures of pyrite and ferrihydrite on the basis of an assessment of the PCE with an accuracy of 1 to 15% of total Fe. For mixtures of pyrite and goethite, the accuracy was less; the contribution of Fe(II) was overestimated by 17–37% of total Fe. This is probably due to the fact that the relationship between the PCE and the Fe(II)/Fe(III) ratio of pyrite:goethite mixtures deviates much more from linearity than that of pyrite:ferrihydrite mixtures (Figure 3a,b). Wilke *et al*. (2001) report a non-linearity of PCE change for binary mixtures of two minerals where both redox state and coordination number change. This is not the case for pyrite and any of the Fe oxyhydroxides investigated, which are all characterized by octahedral coordination (6-coordination) of the Fe. However, Petit *et al*. (2001) and Wilke *et al*. (2001) report that the pre-edge peaks of ferrihydrite, goethite, and haematite are increasingly distorted by extra peak components caused by increased octahedral Fe polymerization, which results in additional compounds contributing to the pre-edge peak at the high-energy end. In accordance with this observation of Petit *et al*. (2001), in our study the PCE was slightly greater for goethite (7115.5 eV) than for ferrihydrite (7114.9 eV). However, the difference of 0.6 eV is close to the energy resolution of the instrument and thus too small for a quantification of ferrihydrite and goethite in binary mixtures of these minerals (Figure 3c). In summary, our results suggest that for soil samples containing inorganic Fe both as Fe(II) (e.g. in pyrite or

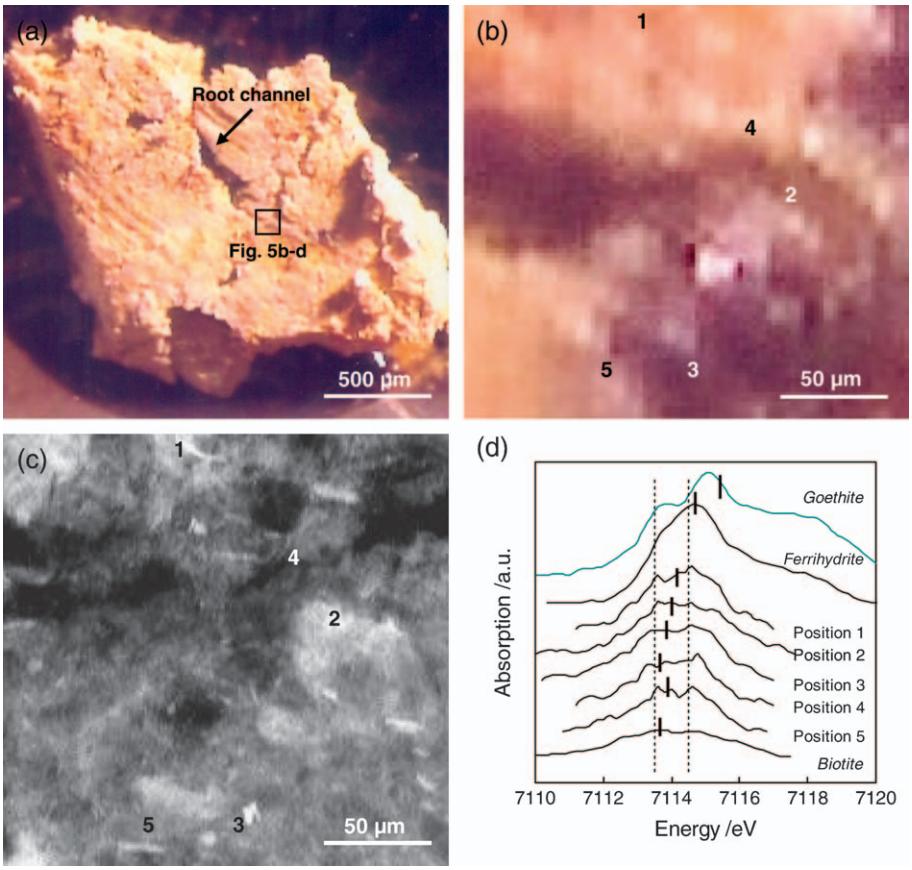

Figure 5 Dissected aggregate taken from the Bg horizon of an epistagnic endogleyic Phaeozem near Freising. (a,b) Photographs taken with an optical microscope, showing (a) the dissected aggregate at 1:25 magnification, (b) the area in the vicinity of a root channel. Fe *K*-edge XANES spectra were taken at positions with Fe enrichment (1,2,3), a position close to the root channel (4), and a position in the aggregate interior with an average Fe content (5). (c) Fe fluorescence map of the region shown in Figure 5(b). (d) Pre-edge peak spectra of positions 1–5. Pre-edge peak centroid energy positions are indicated with solid bars.

Fe(II) silicates) and Fe(III) (e.g. in ferrihydrite and/or goethite), the assessment of the PCE should allow an estimate, but not an accurate quantification, of their Fe(II)/Fe(III) ratio. In our study, the contribution of Fe(II) compounds in mineral mixtures in most cases was considerably overestimated by the PCE approach (Figure 6; empty circles). The situation is even more complicated when organic and inorganic Fe coexist in a sample, which is likely to be the case in topsoil horizons. The PCEs of the organic Fe(II) standards were 0.6 eV less than those of the inorganic Fe(II) standards and 0.6–1.1 eV less than those of Fe(II) minerals (Table 1), which makes a correct Fe(II)/Fe(III) assignment impossible for samples including inorganic and organic Fe(II).

Assessment of the Fe(II)/Fe(III) ratio and quantification of different Fe-bearing compounds in mineral mixtures and soil samples by Linear Combination Fitting

For different synthetic mixtures of Fe-bearing minerals (pyrite, ferrihydrite, and goethite) diluted in quartz, a fairly accurate assessment was achieved of the relative proportion of Fe(II), present as pyrite, and Fe(III), present as ferrihydrite or goethite, when the entire XANES spectrum in the energy range between 7085 eV and 7240 eV was deconvoluted by Linear Combination Fitting (Figure 6; filled circles). The LCF conducted on the pre-edge peak feature yielded less accurate results and overestimated the Fe(II) content in goethite:ferrihydrite mixtures (Table 2). In contrast, with LCF conducted on the entire XANES spectrum the contribution of pyrite to different binary and ternary mixtures of pyrite, ferrihydrite and goethite could be quantified with an accuracy of 1–13% of total Fe and excellent precision (standard error $< 1\%$ of total Fe). This finding indicates that an analysis of the Fe *K*-edge XANES spectrum of a soil sample by LCF provides a fair estimate of the contribution of Fe(II) and Fe(III) species to its total Fe content. Moreover, according to our results a fair estimate of different Fe-bearing phases included in the LCF model is also possible. However, two restrictions must be made. First, in our experiment the Fe(III) oxyhydroxides goethite and ferrihydrite could not be distinguished with LCF conducted on either the entire Fe *K*-edge

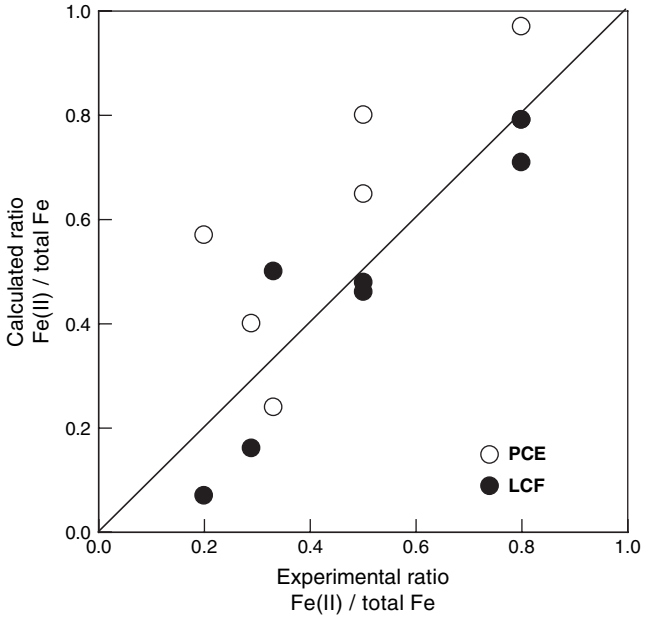

Figure 6 Comparison between the contribution of Fe(II) to total Fe in different diluted mixtures of pyrite, ferrihydrite, and goethite (experiment 2) as calculated by the pre-edge peak centroid energy of the Fe *K*-edge XANES spectrum (PCE) and by Linear Combination Fitting (LCF) conducted on the entire spectrum (7085–7240 eV).

XANES spectrum or its pre-edge feature. This is in line with earlier results of O'Day *et al.* (2004). A higher energy resolution will probably not help in solving the problem of goethite and ferrihydrite discrimination by LCF, because the line widths shown here are core-hole life-time dependent. However, according to Strawn *et al.* (2002), Fe-EXAFS is able to distinguish ferrihydrite, goethite and haematite. Second, LCF yields accurate results only if all potentially relevant Fe phases in a sample are known and their spectra are available as standard substances. This may be of minor concern when samples of subsoil horizons are investigated, where Fe is mainly present as well-defined Fe silicate (e.g. biotite), Fe sulphide (e.g. pyrite), and Fe oxyhydroxide minerals (e.g. ferrihydrite, goethite, haematite), which are available as pure synthetic minerals. However, at the moment it remains open whether the Fe *K*-edge XANES of Fe oxyhydroxides of Fe-phyllosilicates formed in soils, which often are impure (e.g. Murad & Schwertmann, 1988), are similar to those of the same mineral synthesized in the laboratory. In organic horizons, however, a significant part of total Fe is probably present as organically complexed Fe, with the exact composition and structure of the organic binding partners being unknown. It is commonly accepted that organically bound Fe in soils is mainly bound to carboxylate groups of deprotonized fulvic or low-molecular weight acids such as formate, acetate, malate, citrate, and – most important – oxalate (Pohlman & McColl, 1988; Lundström *et al.*, 2000), which justifies our choice of commercially available Fe(II) and Fe(III) oxalate as model compounds for organically bound soil Fe for deconvoluting Fe-XANES pre-edge peak spectra of organic topsoil horizons by LCF.

Fe speciation in the soils of the Fichtelgebirge

According to the LCF results (Table 4), the iron in the organic topsoil horizons of the Fichtelgebirge soils is dominated by Fe(III) oxyhydroxides (32–54% of total Fe) and organically complexed Fe(III) (33–53% of total Fe), whereas no organically complexed Fe(II), no pyrite and only a small amount of Fe monosulphide was detected. Our results are in line with the predominance of Fe(III) over Fe(II) in Fe complexes with lignocellulosic substrate extracted from wheat straw (Guillon *et al.*, 2003). The increasing proportion of Fe(II) in the organic topsoils with increasing groundwater influence, i.e. from the Cambisol to the Histosol, is obviously exclusively due to an increased contribution of Fe(II) silicate to the total Fe content. With 1.0 g silicate-Fe(II) kg^{-1} soil in the Cambisol Oh horizon, and 0.8 g silicate-Fe(II) kg^{-1} soil in the Planosol and Histosol H2 horizons, the concentration of silicate-bound Fe(II) is fairly similar for all topsoils investigated; in contrast, the concentration of Fe bound in Fe(III) oxyhydroxides decreases strongly with increasing groundwater influence from 5.1 g kg^{-1} in the Cambisol Oh horizon to 1.1 g kg^{-1} in the H2 horizons of the Planosol and the Histosol. It must be noted, however, that the Fe *K*-edge XANES spectra of Fe(III) oxalate and Fe(III) oxyhydroxides are very similar (Figure 2), and thus the discrimination of these compounds by LCF is probably inaccurate.

As for the organic topsoils, the evaluation of the PCE and also the results of the LCF for the subsoil horizons investigated revealed an increasing contribution of Fe(II) to total Fe with increasing groundwater influence from the Cambisol to the Histosol. According to LCF, Fe(III) oxyhydroxides are the dominating Fe minerals in all soils (59–100% of total Fe). However, the concentration of these minerals and also their contribution to the total Fe content of the subsoil decrease strongly from the Cambisol Bw horizon (27 g oxyhydroxide-Fe kg^{-1} soil; 100% of total Fe) to the Planosol Bg (10 g oxyhydroxide-Fe kg^{-1} soil; 86% of total Fe) and the Histosol Cr horizon (6 g oxyhydroxide-Fe kg^{-1} soil; 59% of total Fe). In all subsoils, the concentration of Fe bound in oxyhydroxides as calculated by the LCF was generally much larger than the concentration of dithionite-extractable Fe in the respective horizons (Table 3). The colours of the Planosol Bg horizon (10 YR 6/2) and the Histosol Cr horizon (10 YR 3/2) support the small Fe(III) oxyhydroxide concentration in both horizons as determined with the DCB method. According to the results of the latter, most of the Fe in the Planosol Bg and the Histosol Cr horizons is present as silicate rather than Fe(III) oxyhydroxide. Moreover, experiments conducted by Paul *et al.* (2006) showed that in the water-logged Histosol, permanently anoxic conditions inhibit the formation of Fe(III) oxyhydroxides. The seeming discrepancy between the results of the DCB method and the LCF may be due to the fact that Fe(III)-bearing illites,

vermiculites, and chlorites, which according to Eusterhues *et al.* (2003) are the dominant clay minerals in the soils of the study area, have not been included as predictor variables in the LCF. Iron(III) present in these clay minerals was probably erroneously assigned to Fe(III) bound in oxyhydroxides. Whereas no Fe sulphide was detected by LCF in the Bw horizon of the Cambisol, the Bg horizon of the Planosol and the Histosol Cr horizon both contained about 1.5 g Fe monosulphide kg^{-1} soil. Additionally, in the Cr horizon of the Histosol 3.1 g pyrite kg^{-1} soil are present according to the LCF. The granitic bedrock does not contain a significant amount of sulphur; however, the area has been subject to large atmospheric sulphate deposition during recent decades (Manderscheid *et al*., 2000; Paul *et al*., 2006). Our results indicate that a substantial part of the atmospheric sulphate has been reduced and accumulated not only as organic reduced S, but also as Fe monosulphide and pyrite in the water-logged Histosol, whereas this was not the case in the Cambisol. These findings are consistent with results of a sulphur isotope study conducted in the area by Alewell & Novak (2001) and demonstrate the coupling between the cycling of Fe and S in wetland soils (Brown, 1986).

Potential and limitation of Fe K-edge XANES for the Fe speciation in soils

Our study as well as the results of earlier ones conducted on defined binary and ternary mixtures of different Fe-bearing minerals (e.g. Wilke *et al*., 2001; O'Day *et al*., 2004) showed that with Fe *K*-edge XANES the relative contribution of different mineral classes and groups of organic compounds with different oxidation state of the Fe atom (e.g. Fe(II) sulphides versus Fe(III) oxyhydroxides; Fe(II)-organic complexes versus Fe(III)-organic complexes) can be estimated roughly by calculation of the PCE and fairly well by applying LCF to the entire XANES spectrum. At present, LCF conducted on the XANES spectrum in an energy range between 7085 and 7240 eV allows the quantification of specific minerals and organic compounds in soils approximately, but not accurately. The accuracy of the results of the LCF procedure is strongly affected by the correctness of the applied set of predictor variables. Thus for mineral soil horizons, a qualitative *a priori* identification of candidate Fe phases which are likely to be present in the soil and thus should be included as independent variables in the LCF is recommended. This can be done by compiling available information about the mineralogical composition of the parent material from geologic surveys, by previous investigation of the samples of interest with (μ-)XRD or (μ-)XRF. However, the situation is complicated by the circumstance that most soils probably contain non-stoichiometric or impure Fe compounds which are not present in the parent material, but have been formed by weathering and pedogenesis (secondary minerals, humic compounds). In LCF exercises, these constituents are probably only approximately represented by laboratory-synthesized Fe compounds or mineral specimens obtained from bedrock. Therefore an exact quantification of different Fe phases in soils by Fe *K*-edge XANES will probably always remain difficult. Nevertheless, our study yielded a reasonable Fe speciation for all soil horizons investigated. Moreover, it revealed a systematic effect of increasing groundwater influence on the Fe speciation in the topsoil and the subsoil of a forest soil toposequence: the contribution of Fe(II) compounds increased at the expense of Fe(III) compounds. It thus demonstrates the considerable potential of Fe *K*-edge XANES for the determination of Fe speciation in soils despite its present problems and restrictions.

Potential of Fe K-edge μ-XANES for the Fe speciation of soil microsites

A particularly intriguing application of Fe *K*-edge μ-XANES in soil science has been demonstrated in experiment 4. Here, the Fe speciation of several regions in a dissected soil aggregate was shown to be different on a micron or submicron scale. The results of experiment 4 show that focused Fe *K*-edge XANES allows the quantification of Fe(II) and Fe(III) and different Fe compounds in mottles, concretions, aggregates, and edges of root channels. This opens new perspectives in soil research. In our particular example, μ-XANES at the Fe *K*-edge in different regions of the dissected aggregate confirmed analytically the visual impression that the rusty mottle at position 1 was enriched in Fe(III) oxyhydroxides. In contrast, the smaller PCE of the region studied close to the root channel indicates that this region was depleted in Fe(III) oxyhydroxides and perhaps also in Fe(III) clay minerals (Ernstsen *et al*., 1998) relative to the average aggregate interior. This result also supported the visual impression obtained for many aggregates in soil horizons with stagnic properties: their surfaces, particularly the edges of root channels, are bleached compared to the aggregate interior due to preferential dissolution of Fe(III) and Mn(IV) oxyhydroxides as a result of the lower redox potential (anaerobic decomposition of roots and root exudates; Bloomfield, 1950; Blume, 1968).

Conclusions

With Fe *K*-edge XANES, the proportion of Fe(II) and Fe(III) and the contribution of different Fe compounds in soil samples and soil aggregates can be quantified approximately. A quick estimation of the contribution of Fe(II) and Fe(III) in a sample is possible by comparing the energy of its pre-edge peak centroid with those of reference compounds; a more accurate assessment of different Fe-bearing compounds is possible with a deconvolution of the entire spectrum by Linear Combination Fitting.

At the moment, Fe *K*-edge XANES can fairly well estimate the relative contribution of different mineral classes and groups of organic compounds with different oxidation states of

the Fe atom (e.g. Fe sulphides, Fe oxyhydroxides, Fe(II)- and Fe(III)-organic complexes) in mineral mixtures and soil samples, but fails to quantify specific Fe oxyhydroxides (e.g. ferrihydrite, goethite, and haematite) or distinct Fe-organic compounds.

A combination of μ-XRF and μ-XANES allows the speciation of Fe in different micron or submicron regions of intact or dissected soil aggregates (e.g. aggregate surface, root channel edge, concretion, mottle, average aggregate interior).

Acknowledgements

We gratefully acknowledge the help of Professor Schwertmann (Technische Universität München), Dr Haubrich (Technische Universität Dresden), and Dr Scheinost (Forschungszentrum Rossendorf) for providing mineral specimens. We want to thank Ms G. Harrington for conducting the wet-chemical Fe analyses and Professor Schwertmann and two anonymous reviewers for substantially improving the paper by valuable comments and suggestions. The study was funded by the European Synchrotron Radiation Facility (proposals ME-944; ME-1093).

References

Alewell, C. & Novak, M. 2001. Spotting zones of dissimilatory sulfate reduction in a forested catchment: the ^{34}S-^{35}S approach. *Environmental Pollution*, **112,** 369–377.

Bajt, S., Sutton, S.R. & Delaney, J.S. 1994. X-ray microprobe analysis of iron oxidation states in silicates and oxides using X-ray absorption near edge structure (XANES). *Geochimica et Cosmochimica Acta*, **58,** 5209–5214.

Barrett, R., Kaulich, B., Salomé, M. & Susini, J. 2000. Current status of the Scanning X-ray microscope at the ESRF. In: *X-Ray Microscopy: 6th International Conference. August 2–6, 1999, Berkeley, CA* (eds W. Meyer-Ilse, T. Warwick & D. Attwood), p. 458. American Institute of Physics, Melville, NY.

Bloomfield, C. 1950. Some observations on gleying. *Journal of Soil Science*, **1,** 205–211.

Blume, H.P. 1968. Zum Mechanismus der Marmorierung und Konkretionsbildung in Stauwasserböden. *Zeitschrift für Pflanzenernährung, Düngung, Bodenkunde*, **119,** 124–134.

Blume, H.P. & Schwertmann, U. 1969. Genetic evaluation of profile distribution of aluminum, iron, and manganese oxides. *Soil Science Society of America Proceedings*, **33,** 438–445.

Bonnin-Mosbah, M., Métrich, N., Susini, J., Salomé, M., Massare, D. & Menez, B. 2002. Micro X-ray absorption near edge structure at the sulfur and iron K-edges in natural silicate glasses. *Spectrochimica Acta*, **B 57,** 711–725.

Brown, K.A. 1986. Formation of organic sulphur in anaerobic peat. *Soil Biology and Biochemistry*, **18,** 131–140.

Cornell, R.M. & Schwertmann, U. 1996. *The Iron Oxides*. VCH, Weinheim, Germany.

Delaney, J.S., Dyar, M.D., Sutton, S.R. & Bajt, S. 1998. Redox ratios with relevant resolution; solving an old problem using the synchrotron microXANES probe. *Geology*, **26,** 139–142.

Dyar, M.D., Delaney, J.S. & Sutton, S.R. 2001. Fe XANES spectra of iron-rich micas. *European Journal of Mineralogy*, **13,** 1079–1098.

Dyar, M.D., Gunter, M.D., Delaney, J.S., Lanzarotti, A. & Sutton, S.R. 2002. Systematics in the structure and XANES spectra of pyroxenes, amphiboles, and micas as derived from oriented single crystals. *Canadian Mineralogist*, **40,** 1375–1393.

Ernstsen, V., Gates, W.P. & Stucki, J.W. 1998. Microbial reduction of structural iron in clays: a renewable source of reduction capacity. *Journal of Environmental Quality*, **27,** 761–766.

Eusterhues, K., Rumpel, C., Kleber, M. & Kögel-Knabner, I. 2003. Stabilisation of soil organic matter by interactions with minerals as revealed by mineral dissolution and oxidative degradation. *Organic Geochemistry*, **4,** 1591–1600.

Galoisy, L., Calas, G. & Arrio, M.A. 2001. High-resolution XANES spectra of iron in minerals and glasses: structural information from the pre-edge region. *Chemical Geology*, **174,** 307–319.

Goeman, U.E.H. 1972. Mineralbestand und petrographische Kennzeichung der dem variskischen Fichtelgebirgsgranit vorgelagerten Granitstöcke Reut bei Gefrees, Waldstein (mit Epprechtstein) und Kornberg. *Mineralogy and Petrology*, **18,** 203–242.

Guillon, E., Merdy, P. & Aplincourt, M. 2003. Molecular scale speciation of first-row transition elements bound to ligneous material by using X-ray absorption spectroscopy. *Chemistry – a European Journal*, **9,** 4479–4484.

Holmgren, G.G.S. 1967. A rapid citrate-dithionite extractable iron procedure. *Soil Science Society of America Proceedings*, **31,** 210–211.

LaForce, M.J. & Fendorf, S. 2000. Solid phase iron characterization during common selective sequential extractions. *Soil Science Society of America Journal*, **64,** 1608–1615.

Lundström, U.S., van Breemen, N. & Bain, D. 2000. The podzolization process. A review. *Geoderma*, **94,** 91–107.

Manderscheid, B., Schweisser, T., Lischeid, G., Alewell, C. & Matzner, E. 2000. Sulfate pools in the weathered substrata of a forested catchment. *Soil Science Society of America Journal*, **64,** 1078–1082.

Mehra, O.P. & Jackson, M.L. 1960. Iron oxide removal from soils and clays by a dithionite-citrate system buffered with sodium bicarbonate. *Clays and Clay Minerals*, **7,** 317–327.

Murad, E. & Schwertmann, U. 1988. The characterization of poorly crystalline Si-containing natural iron oxides by Mössbauer spectroscopy. *Hyperfine Interactions*, **41,** 835–838.

O'Day, P.A., Rivera, N., Root, R. & Carroll, S.A. 2004. X-ray absorption spectroscopic study of Fe reference compounds for the analysis of natural sediments. *American Mineralogist*, **89,** 572–585.

Paul, S., Küsel, K. & Alewell, C. 2006. Reduction processes in forest wetlands: tracking down heterogeneity of source/sink functions with a combination of methods. *Soil Biology and Biochemistry*, **38,** 1028–1039.

Petit, P.E., Farges, F., Wilke, M. & Solé, V.A. 2001. Determination of the iron oxidation state in Earth materials using XANES pre-edge information. *Journal of Synchrotron Radiation*, **8,** 952–954.

Pohlman, A.A. & McColl, J.G. 1988. Soluble organics from forest litter and their role in metal dissolution. *Soil Science Society of America Journal*, **52,** 265–271.

Prietzel, J., Thieme, J., Neuhäusler, U., Susini, J. & Kögel-Knabner, I. 2003. Speciation of sulphur in soils and soil particles by X-ray spectromicroscopy. *European Journal of Soil Science*, **54,** 423–433.

Scheinost, A. & Schwertmann, U. 1999. Color identification of iron oxides and hydroxysulfates: use and limitations. *Soil Science Society of America Journal*, **63,** 1463–1471.

Schwertmann, U. 1964. Differenzierung der Eisenoxyde des Bodens durch Extraktion mit Ammoniumoxalat-Lösung. *Zeitschrift für Pflanzenernährung, Düngung, Bodenkunde*, **105,** 194–203.

Schwertmann, U. 1993. Relationships between iron oxides, soil color, and soil formation. In: *Soil Color*. *SSSA Special Publication 31* (eds J.M. Bigham & E.J. Cziolkosz), pp. 51–69. Soil Science Society of America, Madison, Wisconsin.

Schwertmann, U. & Cornell, R.M. 1991. *Iron Oxides in the Laboratory: Preparation and Characterization*. VCH, Weinheim, Germany.

Schwertmann, U. & Lentze, W. 1966. Bodenfarbe und Eisenoxidform. *Zeitschrift für Pflanzenernährung, Düngung, Bodenkunde*, **115,** 209–214.

Schwertmann, U., Schulze, D.G. & Murad, E. 1982. Identification of ferrihydrite in soils by dissolution kinetics, differential X-ray diffraction, and Mössbauer spectroscopy. *Soil Science Society of America Journal*, **46,** 869–875.

Schwertmann, U. & Taylor, R.M. 1989. Iron oxides. In: *Minerals in the Soil Environment* (eds J.B. Dixon & S.B. Weed), pp. 379–437. Soil Science Society of America, Madison, WI.

Strawn, D., Doner, H., Zavarin, M. & McHugo, S. 2002. Microscale investigation into the geochemistry of arsenic, selenium, and iron in soil developed in pyritic shale materials. *Geoderma*, **108,** 237–257.

Waychunas, G.A., Apted, J.M. & Brown, G. 1983. X-ray K-edge absorption spectra of Fe minerals and model compounds: near edge structure. *Physics and Chemistry of Minerals*, **10,** 1–9.

Westre, T.E., Kennepohl, P., DeWitt, J.G., Hedman, B., Hodgson, K.O. & Solomon, E.I. 1997. A multiplet analysis of Fe K-edge 1s → 3d pre edge features of iron complexes. *Journal of the American Chemical Society*, **119,** 6297–6314.

Wilke, M., Farges, F., Petit, P.E., Brown, G.E. & Martin, F. 2001. Oxidation state and coordination of Fe in minerals: an Fe K-XANES spectroscopic study. *American Mineralogist*, **86,** 714–730.

WRB (IUSS Working Group WRB) 2006. *World Reference Base for Soil Resources 2006*, 2nd edn. World Soil Resources Reports, 103. FAO, Rome.